communications earth & environment

ARTICLE

https://doi.org/10.1038/s43247-021-00274-9 OPEN

Large calcium isotope fractionations by zeolite minerals from Iceland

Claire J. Nelson [1✉], Andrew D. Jacobson[1], Gabriella D. Kitch [1] & Tobias B. Weisenberger [2]

Zeolites are secondary tectosilicates produced during the hydrothermal alteration of basalt. The minerals serve as major sinks of calcium, which readily exchanges with calcium from surrounding groundwater. However, no studies have specifically investigated the calcium isotope geochemistry ($\delta^{44/40}$Ca) of zeolites. Here, we report $\delta^{44/40}$Ca values for zeolites from East Iceland, where the minerals form during progressive burial of the lava pile. The zeolites show a $\delta^{44/40}$Ca range of 1.4‰, which strongly correlates with average mineral calcium-oxygen bond lengths. As this correlation appears most consistent with equilibrium isotope partitioning, our findings point toward developing a novel geothermometer for studying low-grade basalt metamorphism. The results also have significance for using calcium isotopes to trace basalt weathering, including its role in long-term climate regulation and application in carbon capture and storage, a leading strategy for mitigating anthropogenic climate change.

[1] Department of Earth and Planetary Sciences, Northwestern University, Evanston, IL, USA. [2] Breiðdalsvík Research Centre, University of Iceland, Breiðdalsvík, Iceland. ✉email: clairenelson2021.1@u.northwestern.edu

Calcium (Ca), the fifth most abundant element in the Earth's crust[1], plays a key role in regulating climate over geologic timescales[2,3] and is essential for biological processes, such as biomineralization, plant growth, and cellular regulation[4,5]. Due to the ubiquitous occurrence of Ca in Earth and extraterrestrial materials, as well as major geochemical cycles, stable Ca isotope ratios have emerged as a promising tool for investigating processes in geochemistry, cosmochemistry, biology, and archaeology[6,7]. Calcium isotope ratios are reported in delta notation as $\delta^{44/40}Ca_{smp}$ (‰) $= [(^{44}Ca/^{40}Ca)_{smp}/(^{44}Ca/^{40}Ca)_{std} - 1] \times 1000$, where *smp* refers to the sample and *std* refers to the normalizing standard, which in this study is OSIL Atlantic Seawater or ASW ($\delta^{44/40}Ca_{ASW} = 0$‰).

In the ongoing effort to develop and apply the $\delta^{44/40}Ca$ tracer, research has focused on quantifying mechanisms that fractionate isotopes according to their masses and produce isotopic offsets (Δ) between related Ca-bearing reservoirs, i.e., $\Delta^{44/40}Ca_{a-b} = \delta^{44/40}Ca_a - \delta^{44/40}Ca_b$. Differentiating between kinetic and equilibrium isotope effects during mineral formation is particularly essential for implementing Ca isotopes as paleoenvironmental or temperature proxies[8–10]. Most studies aimed at understanding Ca isotope fractionation during mineral precipitation have focused on calcite ($CaCO_3$) formation at low temperatures (<30 °C) characterizing the Earth's surface. Here, kinetic isotope effects[11–17] cause calcite to preferentially incorporate lighter Ca isotopes from solution with $\Delta^{44/40}Ca_{cal-sol}$ on the order of −1‰ to −2‰[6]. Theory predicts that higher temperatures should promote equilibrium effects and minimize isotopic offsets ($\Delta^{44/40}Ca_{cal-sol} \approx 0$‰) during calcite formation[13,16,18]; however, only a handful of natural calcites precipitated at elevated temperatures have been measured[19–22]. In parallel, some studies examining silicate mineral formation at high temperatures characterizing the solid Earth have attributed $\delta^{44/40}Ca$ variability to equilibrium isotope partitioning[23,24], driven by differences in Ca–O bonding conditions[9,10]. However, discrepancies between measured inter-mineral $\Delta^{44/40}Ca$ of high-temperature silicates and ab initio model predictions of equilibrium Ca isotope offsets have been interpreted as evidence for mostly kinetic control[25,26].

Missing from Ca isotope fractionation theory is an understanding of mechanisms that produce $\delta^{44/40}Ca$ variability during mineral formation at temperatures bridging the surface and solid Earth. Intermediate temperatures in the range of ~30–200 °C characterize many hydrothermal systems, which represent key interfaces linking surficial geochemical cycles and solid Earth processes. Studies have used Ca isotopes to examine mid-ocean ridge hydrothermal systems[19,27,28], seafloor weathering and oceanic lithosphere subduction[22], continental hydrothermal systems[20], and water–rock interactions in pilot studies of mineral carbonation of basalt, which is a leading carbon capture and storage (CCS) strategy[29,30]. Application of the Ca isotope tracer to these and other intermediate temperature systems requires a thorough examination of all secondary minerals that may fractionate Ca isotopes and contribute to the $\delta^{44/40}Ca$ values of circulating waters. In addition, a better understanding of both equilibrium and kinetic effects on Ca isotope fractionation at intermediate temperatures is essential for improving knowledge about Ca isotope cycling and identifying novel applications for the $\delta^{44/40}Ca$ tracer.

Hydrothermal alteration commonly leads to the formation of zeolites[31,32]. Zeolite mineral structures comprise frameworks of linked Si- or Al-O tetrahedra, creating voids and channels that contain H_2O, Ca, and other cations, which are readily exchangeable[33–35]. The minerals serve as sizeable Ca^{2+} sinks during low-grade metamorphism[36–42]. In basaltic settings such as Iceland, equilibrium-controlled ion-exchange reactions with zeolites strongly regulate Ca^{2+} concentrations in natural hydrothermal waters[43,44], as well as those produced in CCS experiments[45–48]. Calcium cycling during basalt weathering in subsurface hydrothermal systems also plays a major role in regulating Earth's long-term carbon cycle[49–51]. Moreover, owing to their properties as ion-exchangers, absorbents, molecular sieves, and catalysts[52], zeolites have numerous environmental, industrial, and medical applications, including drinking water purification[53–55], nuclear waste management[56,57], contaminant transport mitigation[58–60], automotive emission reduction[61], and cancer treatment[62].

Nonetheless, despite the widespread occurrence and applicability of zeolites, their Ca isotope geochemistry has been neglected. Only one study has reported Ca isotope data for zeolites[21]. Coexisting heulandite and stilbite from Iceland are isotopically lighter and heavier, respectively, relative to basalt. Icelandic hydrothermal water and calcite also have $\delta^{44/40}Ca$ values higher than basalt[21]. Heavy calcite is highly unusual because most carbonate minerals form kinetically and incorporate lighter isotopes relative to their Ca source reservoir[13,17,63]. Uptake of lighter Ca isotopes during zeolitization may elevate the relative abundance of heavier Ca isotopes in hydrothermal waters from which calcite precipitates[21], but no systematic understanding has been established.

To better understand the Ca isotope geochemistry of zeolites, we used a high-precision thermal ionization mass spectrometry (TIMS) method to measure $\delta^{44/40}Ca$ values of six zeolite mineral species. We also analyzed bulk basalt, primary mineral separates, and calcite. Specimens were collected from the Berufjörður–Breiðdalur region of East Iceland, which is a type-locality for the zeolitization of basaltic lava flows due to burial metamorphism[64]. Here, increasing temperature with depth below the surface of the lava pile has generated distinct zeolite zones where two zeolite mineral types, referred to as coindex mineral pairs[64], distinctly form and thus are diagnostic of each depth zone (Fig. 1). Depth-controlled zeolite zones have been identified worldwide in active geothermal systems[37,44,65], as well as extinct systems now exposed at the surface[32,38,41,66,67]. We report a large range of zeolite $\delta^{44/40}Ca$ values, which is best explained by equilibrium isotope partitioning, given a strong observed correlation with Ca–O bond lengths. Our findings point the way for developing entirely new tools for investigating low-grade basalt alteration. They also broadly illustrate how future efforts focused on the Ca isotope geochemistry of zeolites could have implications for numerous other topics, such as understanding the compositional evolution of hydrothermal waters, quantifying elemental cycling in the oceans, and improving CCS strategies.

Geologic setting

Iceland is an exposed section of the Atlantic mid-ocean ridge overlying a mantle plume, which has caused extensive rifting and volcanism over the past 50–60 Myr[68]. Rocks increase in age away from the active rift zone, with the oldest rocks at the edges of Iceland dating to ~16 Ma[69]. Samples analyzed in this study were collected from Berufjörður–Breiðdalur region described in detail by Walker (1960) (Fig. 1). Successive eruptions of a Tertiary volcano supplied lava that piled to a minimum total thickness of ~2000 m at the eastern end[64,70,71]. The central volcano comprises highly altered rhyolite, while the flows are predominantly tholeiitic basalt, with lesser amounts of olivine basalt[64,71]. Within ~1 Myr after the eruptions ceased, heat from burial, as well as the volcanic center and associated dike swarms, extensively zeolitized the lava pile, filling up to 90% of the primary porosity[38,64,70,72]. Pleistocene glacial erosion carved deep valleys and fjords into the lava pile and exposed the top ~1000 m of the altered sequence, where the depth-controlled zeolite zones are clearly delineated

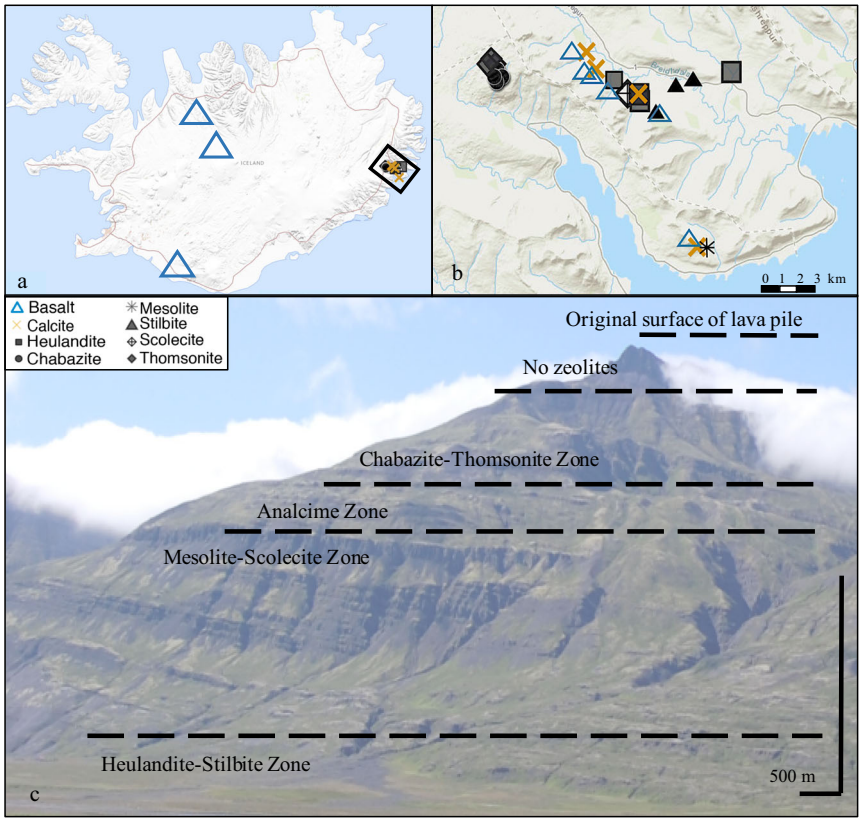

Fig. 1 Map of Iceland showing sample locations. a Mineral separates were obtained from basalts sampled throughout Iceland. The Berufjörður–Breiðdalur region of East Iceland is outlined. **b** Sampling locations of bulk rocks, calcite, and zeolites collected from the main region of study. **c** Zeolite sampling locations correspond to different elevations or depths below the original surface of the lava pile. Depth-controlled zeolite zones, adapted from Walker (1960), are overlain on a photograph of the Berufjörður volcanic sequence taken from the north.

and accessible above sea level (Fig. 1). The shallowest zone studied here is the chabazite–thomsonite zone (~30–70 °C), followed by the mesolite–scolecite zone (~70–90 °C) and the stilbite–heulandite zone (~90–150 °C), which reaches a maximum depth of ~1500 m below the top of the lava pile[31,39,64,73].

Results

Bulk basalt and primary minerals. Table 1 presents elemental and Ca isotope data for bulk basalt and primary mineral separates. Bulk basalt samples from the Berufjörður–Breiðdalur region yield an average $\delta^{44/40}$Ca of -1.04 ± 0.08‰ ($2\sigma_{SD}$, $n = 5$), which agrees well with the average of -1.06 ± 0.02‰ ($2\sigma_{SD}$, $n = 6$) for basalt sampled from other regions throughout Iceland[21]. The primary minerals have a narrow range of $\delta^{44/40}$Ca values, which bracket those for bulk basalt. Olivine has the highest average $\delta^{44/40}$Ca (-1.02 ± 0.14‰, $2\sigma_{SD}$, $n = 3$), followed by clinopyroxene (-1.05 ± 0.06‰, $2\sigma_{SD}$, $n = 3$), apatite (-1.12 ± 0.06‰, $2\sigma_{SD}$, $n = 3$), and plagioclase (-1.14 ± 0.04‰, $2\sigma_{SD}$, $n = 3$).

Calcite. Table 1 presents elemental and Ca isotope data for calcite samples. The average $\delta^{44/40}$Ca equals -0.80 ± 0.20‰ ($2\sigma_{SD}$, $n = 4$), which is similar to the average of -0.79 ± 0.34‰ ($2\sigma_{SD}$, $n = 13$) for zeolite-zone calcite reported in Jacobson et al. (2015). Calcite consistently has higher $\delta^{44/40}$Ca than basalt and primary minerals.

Zeolites. Table 2 provides elemental and Ca isotope data for bulk zeolites. Stilbite has the highest average $\delta^{44/40}$Ca (-0.72 ± 0.24‰,

Table 1 Elemental and Ca isotope data for bulk basalt, primary mineral separates, and calcite.

Sample ID	Ca (μmol/g)	Na (μmol/g)	Sr (nmol/g)	Mg (μmol/g)	$\delta^{44/40}$Ca (‰)
Bulk basalt					
ILR_D_6	1997	701	2845	1582	−1.00
ILR_D_13	1833	656	3168	1275	−1.10
ILR_12_f	1280	792	3145	1008	−1.02
ILR_12_l	1748	668	3049	1371	−1.02
ILR_12_m	1723	759	2894	1201	−1.05
Plagioclase					
ILR_PL_16	3206	437	2139	69.1	−1.12
ILR_SJ_22	2800	753	8084	47.5	−1.15
ILR_SV_2	3212	460	2293	62.7	−1.16
Clinopyroxene					
ILR_PL_16	3405	134	299	3633	−1.03
ILR_SJ_22	4023	141	560	3369	−1.05
ILR_SV_2	3873	94.7	189	3260	−1.08
Apatite					
ILR_PL_16	3162	448	2384	158	−1.09
ILR_SJ_22	2390	811	7883	56.5	−1.14
ILR_SV_2	3105	539	2589	185	−1.14
Olivine					
ILR_PL_16	344	51.9	119	9269	−0.95
ILR_SJ_22	2416	127	497	4605	−1.08
ILR_SV_2	900	51.4	104	6878	−1.03
Calcite					
ILM_C_15	9182	—	140	0.72	−0.66
ILM_C_35	9120	—	2428	3.37	−0.89
ILM_C_44	8802	—	1916	23.6	−0.86 (−0.87)
ILM_C_49	8710	—	174	1.04	−0.80

Duplicate analyses are shown in "()". Elements not detected are marked with "—".

Table 2 Elemental and Ca isotope data for bulk zeolite minerals.

Sample ID	Ca (μmol/g)	Na (μmol/g)	Sr (nmol/g)	Si (μmol/g)	Al (μmol/g)	$\delta^{44/40}$Ca (‰)
Heulandite						
HD_1	1243	426	23,551	9706	3130	−1.74
HD_11	1350	468	26,254	9713	3209	−1.72
HD_18	1219	456	24,593	9753	3062	−1.69
HD_23	1280	447	26,143	9674	3107	−1.90
HD_28	1305	429	21,123	—	—	−2.00
Chabazite						
CZ_54	1698	163	17,815	7995	3662	−1.72
CZ_56b	1644	216	11,681	8211	3550	−1.48
CZ_61	1640	317	12,881	8240	3621	−1.49
CZ_62	1734	199	18,117	8003	3729	−1.62
Thomsonite						
TM_57	1368	328	51.5	9293	3240	−0.91
TM_58	1415	474	38.1	9263	3211	−0.87
TM_63	1412	680	120	8960	3483	−1.04
Stilbite						
SB_17	1417	161	41.1	9796	2946	−0.62
SB_69	1401	157	95.5	9543	2750	−0.68
SB_73	1462	209	535	9651	3015	−0.85
Mesolite						
MS_50	1786	1689	3951	7183	5604	−1.78
Scolecite						
SC_3	1857	80.2	53.7	7940	4907	−0.84

Analyses not made due to limited sample sizes are marked with "—".

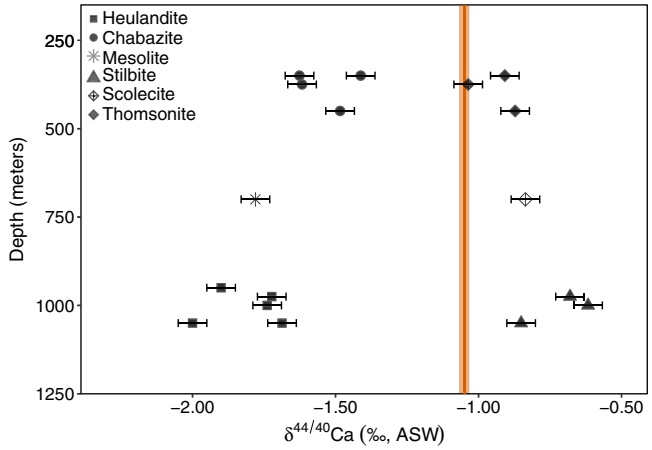

Fig. 2 Zeolite $\delta^{44/40}$Ca versus burial depth. $\delta^{44/40}$Ca of bulk zeolites versus approximate burial depth in the Berufjörður-Breiðdalur region[64]. The orange line shows the average value for all basalts analyzed here and by Jacobson et al. (2015), with the width encompassing the standard deviation (−1.05 ± 0.06‰, $2\sigma_{SD}$, $n = 11$). Error bars show external reproducibility (±0.05‰, $2\sigma_{SD}$).

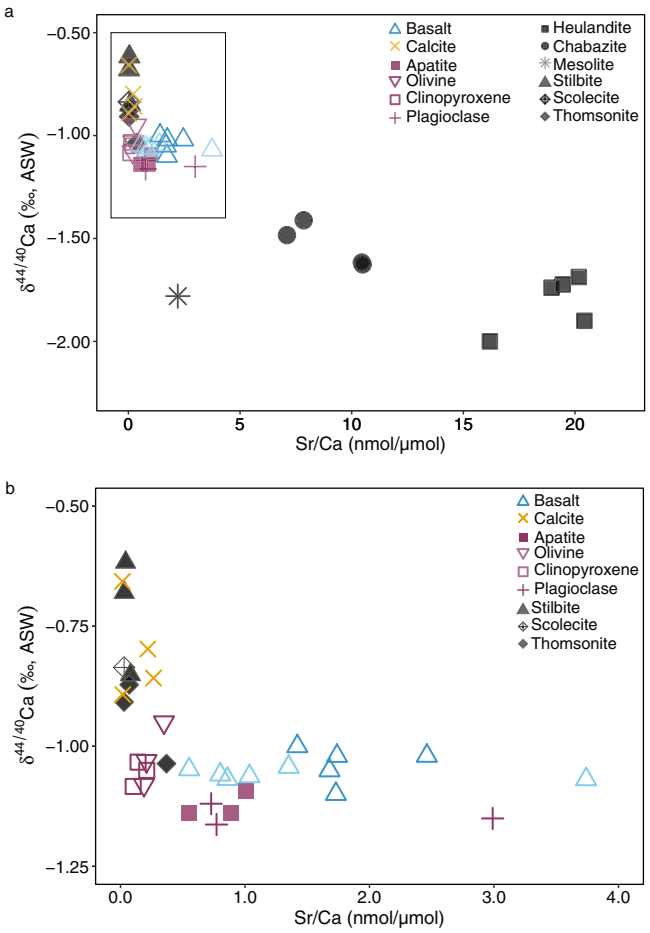

Fig. 3 $\delta^{44/40}$Ca versus Sr/Ca for primary minerals, bulk basalt, calcite, and zeolites. a Ca isotope measurements of all samples. Symbol size is larger than the external reproducibility (±0.05‰, $2\sigma_{SD}$). **b** Inset from panel (**a**) includes basalt from the Berufjörður-Breiðdalur region (dark blue triangles), as well as basalt from previous studies (light blue triangles)[21].

$2\sigma_{SD}$, $n = 3$), followed by scolecite (−0.84‰, $n = 1$), thomsonite (−0.94 ± 0.18‰, $2\sigma_{SD}$, $n = 3$), chabazite (−1.58 ± 0.22‰, $2\sigma_{SD}$, $n = 4$), mesolite (−1.78‰, $n = 1$), and heulandite (−1.81 ± 0.28‰, $2\sigma_{SD}$, $n = 5$). $\delta^{44/40}$Ca for stilbite and heulandite agree with previously reported values[21].

Discussion

Controls on zeolite $\delta^{44/40}$Ca: kinetic isotope effects. A striking observation is that for each zeolite zone[64], coindex pairs have contrasting $\delta^{44/40}$Ca that bracket basalt, with one mineral lower and the other higher (Fig. 2). Relative to basalt, the zeolites chabazite, mesolite, and heulandite have low $\delta^{44/40}$Ca, while their respective pairs (thomsonite, scolecite, and stilbite) have high $\delta^{44/40}$Ca. Chabazite, mesolite, and heulandite represent some of the isotopically lightest minerals thus far measured[6,26,74], neglecting those that host appreciable ^{40}Ca additions from the radioactive decay of ^{40}K[75]. The data provide good evidence that zeolites fractionate Ca isotopes, as bulk basalt and primary mineral separates show effectively no isotopic variability (Fig. 3).

Many studies have shown that kinetic fractionation during mineral precipitation causes preferential uptake of lighter Ca isotopes relative to the main Ca reservoir[11,74]. Other minerals measured thus far with low $\delta^{44/40}$Ca values similar to zeolites are mainly carbonates, which have experienced kinetic fractionation due to either variable precipitation rates[13,14] or biogenic vital effects during mineral growth[74]. Kinetic effects resulting in low $\delta^{44/40}$Ca have also been observed in some high-temperature silicate minerals[25,76,77]. However, unlike carbonates and primary rock-forming silicate minerals, all Ca in zeolites is exchangeable[34]; therefore, it cannot be assumed a priori that kinetic fractionation mechanisms identified for the former minerals apply to zeolites. Kinetic isotope fractionation during mineral precipitation from solution mainly occurs due to incomplete exchange of ions or molecules, when transfer from solution to the solid proceeds more quickly than the reverse reaction[9,11,78]. Calcium ion exchange in zeolite minerals is equilibrium-controlled[34,43], thus implying that forward and backward reaction rates are equal. Nevertheless, we consider below potential transport-related kinetic isotope effects.

Zeolites consist of an aluminosilicate tetrahedral framework, where cations occupy specific exchange sites within void channels[33]. Isomorphic substitution of Al^{3+} for Si^{4+} in the tetrahedra creates a net negative charge in the zeolite framework, which is balanced by the uptake of mono- and divalent cations,

including Ca^{2+}, from the coexisting solution[33]. Thus, coulombic forces related to charge density could in theory kinetically fractionate Ca isotopes due to variable mass-dependent diffusion rates occurring at the mineral–fluid interface or within the zeolite framework itself[11,79–81]. Charge density and distribution, as well as framework topology, control the ease and rate of Ca uptake and diffusion through zeolite frameworks[34,58,82]. Commonly a proxy for charge density, and thus cation-exchange capacity, zeolite Si/Al ratios reflect the anionic field strength that attracts cations into the structure. In general, zeolites with lower Si/Al ratios have higher charge densities and more readily take up cations relative to those with higher Si/Al ratios and lower charge densities[34,83]. If kinetic effects related to rates of Ca uptake or diffusion fractionated Ca isotopes, then a trend between zeolite Si/Al ratios and $\delta^{44/40}$Ca values should exist. However, we observe no trend for the present dataset, suggesting that charge density does not elicit kinetic isotope effects for these minerals (see Fig. S1).

One key point is that basalt represents the initial source of Ca in this system[37,38]. If the occurrence of zeolites with $\delta^{44/40}$Ca higher than basalt was the result of a kinetic fractionation mechanism during mineral formation, then this would require that zeolites with lower $\delta^{44/40}$Ca either precipitate faster or form first, thereby creating an isotopically enriched solution from which zeolites with higher $\delta^{44/40}$Ca later precipitate, as no kinetic fractionation mechanism could result in the preferential uptake of heavier Ca isotopes. Calculations and experiments employing solution chemistry and thermodynamic conditions have been used to predict the progression of zeolitization[84–87], and while petrographic evidence in some locations points to possible chronologic sequences of zeolites[32,40,88,89], studies in Iceland indicate that the coindex pairs form simultaneously under similar conditions[37,38,41,90]. Furthermore, some coindex zeolite pairs analyzed here were intergrown and collected from a single amygdule, suggesting simultaneous precipitation. The absence of clear evidence for kinetically controlled reservoir effects is unsurprising, as all zeolite-bound Ca is extra-framework, with ion-exchange reactions between zeolites and fluids continuing after initial growth of the aluminosilicate frameworks[43,66]. Calculated equilibrium elemental compositions of zeolites, as well as those produced experimentally under equilibrium conditions, agree with geochemical analyses of natural Icelandic zeolites, which strongly indicates that the ion-exchange reactions are equilibrium-controlled[43,44,66]. Because zeolites with identical formation conditions have contrasting $\delta^{44/40}$Ca and the ion-exchange processes governing Ca uptake are equilibrium-controlled, kinetic effects are unlikely to contribute to the $\delta^{44/40}$Ca variations observed here.

Another interesting observation is that zeolites with lower $\delta^{44/40}$Ca also have higher Sr/Ca (Fig. 3). During calcite precipitation, rate-dependent shifts in Ca isotope fractionation and Sr partitioning produce linear correlations between $\delta^{44/40}$Ca values and Sr/Ca ratios[13]; however, the pattern observed in Fig. 3 for zeolites is nonlinear. In general, the understanding achieved for simple ionic solids does not immediately apply to more complex minerals, such as zeolites. Each zeolite studied here has a unique aluminosilicate framework. Incorporation of Sr into chabazite and heulandite, for example, is widely documented to reflect underlying structural characteristics, where zeolite framework topology and local bonding conditions give rise to larger exchange sites that prefer Sr relative to Ca[33,43,91–93]. The trend shown in Fig. 3 provides evidence that structural properties known to control Sr incorporation may also discriminate Ca isotopes as well.

Controls on zeolite $\delta^{44/40}$Ca: equilibrium isotope effects. We deduce that a fractionation mechanism related to mineral-specific Ca bonding conditions likely explains zeolite $\delta^{44/40}$Ca variability. Previous research has shown that Ca isotope fractionation varies as a function of coordination number (CN)[63,94–97], and relationships between $\delta^{44/40}$Ca and Ca–O bond length have been identified for carbonates, phosphates, hydrous minerals, silicates, and aqueous calcium[25,95–98]. Both a function of bond length and CN, bond strength (stiffness) determines isotope fractionation, where stronger bonds preferentially concentrate heavier isotopes[9,99].

The CN of Ca in zeolites can vary widely within each mineral because the minerals support a variety of exchange sites with unique Ca–O bonding conditions[33]. For example, Ca in chabazite could have a CN of 6 or 12 depending on which exchange site Ca occupies (Table 3)[100]. Moreover, within a given zeolite exchange site, Ca can coordinate to either framework oxygens (O_{fmwk}), those composing molecular water also contained within the framework (O_w), or some combination thereof. In general, Ca–O_{fmwk} bonds are considerably longer than Ca–O_w bonds at a given site; thus, Ca–O bond lengths can vary greatly within one individual site, as well as between sites within a single mineral (Table 3). The effect of CN on bond strength is documented for mineral systems where most of the bonds contributing to the CN of Ca have nearly equal lengths, relative to zeolites, which support highly different Ca–O bond lengths[25,95–97]. As the average CN of Ca per zeolite cannot take into account nonuniform bond lengths, the average Ca–O bond length per zeolite likely better approximates bond strength for this particular mineralogical system. Therefore, we calculated an average Ca–O bond length for each unique Ca site and used this as a proxy for the average Ca–O bond length per mineral, assuming Ca is evenly distributed across all potential sites (Table 3).

When zeolite $\delta^{44/40}$Ca values are plotted versus average Ca–O bond length per mineral (Fig. 4), five of the six zeolites studied generate a significant correlation ($R^2 = 0.93$, $p < 0.001$). In general, zeolites with lower $\delta^{44/40}$Ca have longer approximate Ca–O bond lengths, while zeolites with higher $\delta^{44/40}$Ca have shorter approximate Ca–O bond lengths, consistent with equilibrium isotope fractionation theory[9,10]. While CN can adequately predict bond strength for many mineral systems[26,63,74,94,95,97], the observation that stilbite (CN = 8) and scolecite (CN = 7) have nearly identical average Ca–O bond lengths and $\delta^{44/40}$Ca values supports our assumption that bond length better approximates the effect of bond strength on Ca isotope fractionation for zeolites. We suggest that differences in zeolite Ca–O bond energies underlie the trend between $\delta^{44/40}$Ca and bond length shown in Fig. 4, which we interpret as evidence for equilibrium isotope partitioning.

In the context of isotope fractionation between solution and mineral, it is important to consider Ca–O bonding dynamics in the surrounding fluid. Aqueous Ca^{2+} coordinates to water O atoms in coordination or hydration spheres, which have shorter Ca–O bond lengths than zeolites[96]. Icelandic groundwater has higher $\delta^{44/40}$Ca values than zeolites (Fig. 4), consistent with predictions from equilibrium fractionation theory that stronger bonds preferentially concentrate heavier isotopes[8–10]. The exchange of Ca between groundwater and zeolite frameworks involves breaking a certain number of Ca–O_w bonds in the hydration spheres (desolvation) to create Ca–O_{fmwk} bonds[82]. Theoretical studies focusing on calcite have argued that desolvation can elicit kinetic isotope effects due to faster bond breaking of hydration spheres containing lighter Ca isotopes[80,101]. If such a mechanism is applied here, then minerals requiring more bond breaking of hydration spheres (i.e., those comprising fewer Ca–O_w bonds) should preferentially incorporate lighter Ca isotopes. However, this pattern is not observed. For example, heulandite and thomsonite only need to break three

Table 3 Compilation of mineral data used for estimating average mineral Ca–O bond lengths.

Mineral type	Site	Number of Ca–O_w bonds, N_w	Number of Ca–O_{fmwk} bonds, N_{fmwk}	Coordination number for site, CN_s	Average Ca–O_w bond length, l_w (Å)	Average Ca–O_{fmwk} bond length, l_{fmwk} (Å)	Average site Ca–O bond length, l_s (Å)	f_{Ca} in each site	Weighted average mineral Ca–O bond length, L (Å)
Stilbite	Ca-only	8	0	8	2.45		2.45	1	2.45
Mesolite	Ca-only channel	3	4	7	2.34	2.51	2.44	1	2.44
	Na-only channel	2	4	6				0	
Scolecite	Ca-only channel	3	4	7	2.34	2.53	2.45	1	2.45
Thomsonite	Ca-only	2	4	6	2.39	2.52	2.48	0.5	
	Ca or Na	4	4	8	2.56	2.57	2.57	0.5	2.52
Chabazite	C1- Ca-only	0	6	6		3.05	3.05	0.25	
	C2	0	6	6		2.80	2.80	0.25	
	C3	8	4	12	2.36	2.82	2.51	0.25	2.76
	C4- Ca-only	0	8	8		2.67	2.67	0.25	
Heulandite	Ca2	5	3	8	2.63	2.85	2.71	0.333	
	Ca or Na	4	5	9	2.65	2.81	2.74	0.333	2.79
	K3	2	6	8	2.92	2.93	2.93	0.333	

The calculation accounts for different cation bonding sites within tetrahedral frameworks specific to each zeolite, as well as different lengths of Ca–O bonds that vary with the type of O atom participating in the bond. See "Methods" section for equations and supplementary information Table S2 for data sources.

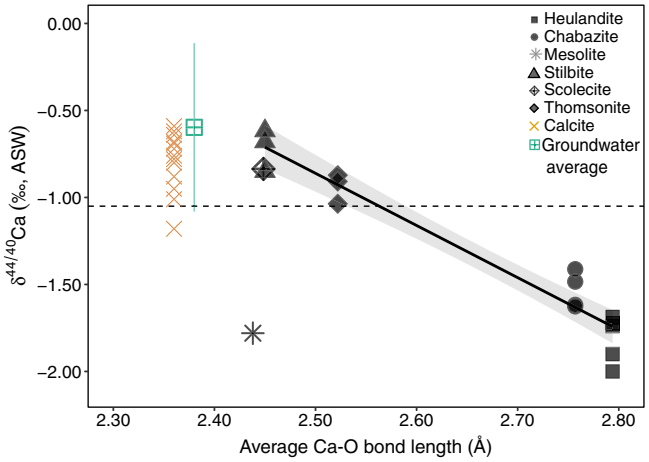

Fig. 4 Zeolite $\delta^{44/40}$Ca versus estimated average Ca–O bond length. Symbol size encompasses the external reproducibility (±0.05‰, $2\sigma_{SD}$). Also shown are $\delta^{44/40}$Ca data for calcite from this study and zeolite-zone calcite from Jacobson et al. (2015), as well as the average of natural groundwaters[21] and pre-injection groundwaters from the CarbFix1 site[29], which circulate through active zeolite zones analogous to the extinct system studied here[65]. Calcite[106,136] and groundwater[96] Ca-O bond lengths are approximate. The black dashed line shows the average value for Icelandic basalt (−1.05‰) determined from this study and Jacobson et al. (2015). Average Ca-O bond lengths and $\delta^{44/40}$Ca values of bulk zeolites strongly correlate ($R^2 = 0.93$, $p < 0.001$), when mesolite is excluded from the regression. The grey shading represents the confidence interval of this regression (see Supplementary information (S1) for details of the statistical model).

to four hydration sphere bonds but show greater apparent fractionations than calcite, which must break at least six hydration sphere bonds, as the mineral supports no Ca–O_w bonds. Stilbite has only Ca–O_w bonds (Table 3), implying an absence of desolvation, yet Icelandic calcite and stilbite have similar $\delta^{44/40}$Ca (Table 2). In addition, chabazite has the least Ca–O_w bonds of all zeolites studied here, but shows higher $\delta^{44/40}$Ca than heulandite. In parallel, heulandite and thomsonite have the same proportions of Ca–O_w bonds relative to total Ca–O bonds, suggesting that these two minerals should desolvate hydration spheres identically, but heulandite has much lower $\delta^{44/40}$Ca values than thomsonite. While more research is needed to constrain relationships between zeolite structural characteristics, desolvation kinetics, and Ca isotope fractionation, our present observations better support an equilibrium isotope effect related to mineral Ca–O bond lengths.

Mesolite is the only exception to the relationship shown in Fig. 4. This zeolite and scolecite support identical Ca-site structures, but the mesolite framework also comprises alternating channels of Ca and Na sites[102,103]. Our bond length estimate assumes that all Ca in mesolite resides in the Ca channel; however, Ca can substitute into the Na channel, where it coordinates to O_{fmwk} with much longer bonds than in the Ca channel[104,105]. For this particular sample, it is possible that a substantial proportion of the Ca occupies the Na channel, where Ca–O_{fmwk} bond lengths are longer than our calculation estimates. Thus, the accumulation of lighter Ca isotopes in the Na channel could explain the sample's lower $\delta^{44/40}$Ca value. Similar observations of bond lengths varying with elemental substitutions have been made for calcite and other silicates, where Mg/Ca ratios discernably correlate with $\delta^{44/40}$Ca[23,26,106].

An alternative explanation is that mesolite experienced kinetic isotope effects. The Ca sites in mesolite and scolecite have identical framework topologies, Ca–O bond lengths, and CNs. Theory for this scenario dictates that contrasting Ca isotope ratios could reflect kinetic isotope effects[26]. However, because precipitation rate effects observed for other types of minerals do not apply to zeolites, which participate in equilibrium-controlled ion exchange after initial precipitation[43,44,66], the exact mechanism that would produce kinetic isotope effects is uncertain. Nevertheless, the data imply that mesolite is the most likely candidate of all zeolites examined here to have experienced kinetic fractionation. If correct, then our observation that mesolite plots off the line in Fig. 4 only supports equilibrium isotope partitioning for the other minerals.

Barring the one mesolite sample, bulk zeolite $\delta^{44/40}$Ca values inversely vary with approximate Ca–O bond lengths. While we interpret this pattern to reflect inter-mineral equilibrium isotope partitioning, more research is needed to better constrain zeolite fractionation mechanisms. The correlation between zeolite Ca–O bond lengths and $\delta^{44/40}$Ca values reported here is consistent with theoretical[23,96–98,107], laboratory[63,95,108], and field studies of other mineral types[24–27,109]. To the best of our knowledge, our study is the first to report such effects for zeolites, as few studies have investigated $\delta^{44/40}$Ca variability in minerals that form in nature at intermediate temperatures. Zeolites with low $\delta^{44/40}$Ca values incorporate more Sr relative to Ca (Fig. 3). As Sr^{2+} has a larger ionic radius than Ca^{2+}, these minerals presumably support larger exchange sites, consistent with Ca isotope evidence that the minerals have longer Ca–O bond lengths. We also note that zeolites appear to fractionate Sr isotopes, with heulandite and stilbite bracketing the composition for bulk basalt[50]. Our overall interpretation is further consistent with an early investigation reporting that fractionation of Li and K isotopes by zeolites during ion exchange is largely equilibrium-controlled[110].

While structural differences between zeolite frameworks adequately explain $\delta^{44/40}$Ca variability, we do note that Ca isotope offsets between the coindex pairs increases with depth (Fig. 2), which counters the expectation that higher temperatures diminish equilibrium isotope fractionation[10]. This only underscores the first-order control of the mineral structure. Each zeolite has a unique framework structure, which gives rise to the positive correlation between the magnitudes of isotopic contrast and Ca–O bond-length differences between the coindex pairs. Zeolite $\delta^{44/40}$Ca values may indirectly relate to formation temperature, as temperature determines which frameworks crystallize as a function of depth[38,64] and structural properties appear to control Ca isotope fractionation (Fig. 4). However, the Ca isotope geochemistry of the minerals could more directly relate to the temperature of coexisting groundwater, as zeolites participate in equilibrium-controlled ion-exchange reactions after formation[38,43,44]. Thus, calcium isotopes could be developed as a proxy for circulating fluid temperature; however, more studies are needed to better elucidate equilibrium versus kinetic controls on fractionation and fully quantify fractionation factors for each mineral relative to solution. Nevertheless, our present findings illustrate the potential for developing an entirely new geothermometer for investigating low-grade basalt metamorphism, as well as probing a diverse range of other environments where zeolites form[111,112].

Controls on hydrothermal water $\delta^{44/40}$Ca. Primary minerals display limited Ca isotope contrast and bracket $\delta^{44/40}$Ca values of bulk basalt (Fig. 3). This confirms previous suggestions that the limited Ca isotope variability of Icelandic basalt is due to a narrow range of primary mineral $\delta^{44/40}$Ca[21]. The source of fluid in the system studied here is meteoric[37,43,72], which implies that its initial $\delta^{44/40}$Ca value is rock-dominated (~−1‰). No evidence exists for

preferential Ca isotope release during primary silicate mineral dissolution for any silicate rock type. Therefore, hydrothermal waters and calcite in Iceland must be driven heavy as a byproduct of secondary light Ca sinks. During hydrothermal alteration of basalt, Ca-bearing zeolites and calcite are the two main sinks of aqueous Ca^{2+} [45,113], with zeolites forming distinctly prior to calcite[38,45,48,90,114]. Smectite and mixed layer clays form before zeolites, but they incorporate little Ca by comparison[38,41,45,65,115]. The low $\delta^{44/40}Ca$ values of chabazite, mesolite, and heulandite indicate that fractionation by zeolites overshadows any effects due to Ca^{2+} adsorption onto clays. If an appreciable amount of clay with low $\delta^{44/40}Ca$ values formed prior to zeolites, then all zeolites would have elevated $\delta^{44/40}Ca$ values, due to a reservoir effect, which is not the observed pattern. Thus, either clays are negligible Ca sinks or they have negligible Ca isotope fractionation factors. Recent research has attributed elevated $\delta^{44/40}Ca$ values in CCS waters to the formation of isotopically light calcite[29], but no such calcite, whether anthropogenic or natural, has been measured in the Icelandic system. However, similar to natural hydrothermal waters[65,116–119], CCS waters are supersaturated with respect to zeolites after periods of CO_2 injection[45,48,90]. While some zeolites do show higher $\delta^{44/40}Ca$ than basalt, the depth trend presented here is clearly asymmetric, where negative fractionations are larger (Fig. 2). Thus, it follows that progressive ion exchange with zeolites would elevate groundwater $\delta^{44/40}Ca$, supporting previous suggestions that uptake of lighter Ca isotopes by zeolites enriches hydrothermal waters in heavier isotopes[21,50,120].

Studies of other groundwater systems have suggested that preferential uptake of lighter Ca isotopes by anhydrite or calcite elevates water $\delta^{44/40}Ca$ values relative to source rocks[19,20,121,122]. Zeolites form ubiquitously at temperatures ranging from ~30 to 150 °C during the hydrous alteration of silicates in many diverse environments[31,123]. Our results emphasize a need to consider Ca uptake by zeolites in studies aimed at understanding the geochemical evolution of natural groundwater, as well as CCS waters monitored during mineral carbonation of basalt[26,29,122,124].

Controls on calcite $\delta^{44/40}Ca$. The overlapping range of calcite and hydrothermal water $\delta^{44/40}Ca$ values in Iceland suggests that $\Delta^{44/40}Ca_{cal-sol}$ is close to 0‰[21], similar to patterns documented in other natural systems, where calcite slowly forms about the state of chemical equilibrium[125,126]. Equilibrium isotope effects appear to control the Ca isotope composition of zeolites, given the strong linear correlation between zeolite Ca–O bond lengths and $\delta^{44/40}Ca$ (Fig. 4). Many hydrothermal calcite samples also have $\delta^{44/40}Ca$ values that closely approach this line, suggesting a similar control by Ca–O bond length. We, therefore, propose that the unusually high $\delta^{44/40}Ca$ of Icelandic hydrothermal calcite reflects the influence of zeolites on hydrothermal water $\delta^{44/40}Ca$. Because calcite samples display a range of $\delta^{44/40}Ca$ values (Fig. 4), it is possible that the lighter calcite samples may have precipitated from hydrothermal waters that isotopically evolved to differing degrees. Alternatively, kinetic isotope effects due to variable precipitation rates may have contributed to the lower $\delta^{44/40}Ca$ of some calcites relative to hydrothermal water. Regardless, it is likely that many Icelandic hydrothermal calcites have $\delta^{44/40}Ca$ values consistent with equilibrium isotope control.

While several studies have identified how variable Ca coordination controls inter-mineral equilibrium isotope partitioning[63,108], few have determined the effects of CN on mineral–fluid Ca isotope partitioning during natural calcite growth[127]. Calcite supports only one Ca site having Ca–O bonds of uniform length;[97,128–130] therefore, unlike zeolites, the CN for calcite adequately approximates bond strength and related isotopic effects. Calcium in calcite coordinates to six O atoms[128]. Thus, calcite has a lower CN than any of the zeolites examined in this study, as well as shorter Ca–O bond lengths. It follows that calcite should have higher $\delta^{44/40}Ca$ than zeolites, which is the relationship observed in Fig. 4. Experimental results and calculations have demonstrated that Ca isotope fractionation during mineral precipitation depends on the CN of mineral Ca, as well as the CN of aqueous Ca^{2+}, which can range from six to ten[80,95–97,131]. Because Icelandic calcite appears to imprint the $\delta^{44/40}Ca$ of hydrothermal waters and plot near the equilibrium-controlled zeolite Ca–O bond-length line, we suggest that aqueous Ca^{2+} in this system likely has a CN of six. Calcite, which has a known CN and a well-constrained Ca–O bond length, shows similar $\delta^{44/40}Ca$ and bond length to Icelandic groundwater; thus, it follows that these reservoirs likely have similar CN. The isotopic offset between water and zeolites further implies that the CN of aqueous Ca^{2+} must be lower than those of zeolites (lowest CN = 7) and more similar to that of calcite (CN = 6). The apparent offset between Ca–O bond lengths for calcite and hydrothermal water (Fig. 4) is likely a consequence of our assumptions, as bond lengths in calcite vary with impurities[97,98], and bond lengths for sixfold coordinated aqueous Ca^{2+} vary with temperature, ion pairing, and fluid ionic strength among other factors[80,95,96,131,132].

Our results suggest that equilibrium-controlled calcite $\delta^{44/40}Ca$ values could be used to identify the CN of aqueous Ca^{2+}, and that laboratory studies able to control the CN of aqueous Ca^{2+} could better constrain equilibrium isotope effects in synthesized calcites. In this context, the equilibrium isotopic offset between calcite and water ($\Delta^{44/40}Ca_{cal-sol}$), which is generally accepted to be ~0‰ given small $\Delta^{44/40}Ca_{cal-sol}$ observed in natural settings where calcite precipitates at or near chemical equilibrium[15,125,126], could be interpreted not only as an absence of kinetic isotope effects but also as an indication that aqueous Ca^{2+} and calcite Ca both have a CN of six. This potentially has implications for various applications of the Ca isotope tracer, as the CN of aqueous Ca^{2+} can vary with ionic strength and temperature[131,133], which could theoretically impact the equilibrium isotope fractionation factor between calcite and water. For example, if fluid Ca^{2+} was coordinated to eight oxygens instead of six (likely resulting in longer bond lengths in the hydration sphere[134]), $\Delta^{44/40}Ca_{cal-sol}$ at equilibrium would be nonzero and positive, resulting in calcite that is enriched in heavier Ca isotopes[95–97]. Further work is needed to explore these ideas; however, our findings provide a valuable perspective on mineral–fluid isotope equilibrium, which could have implications for interpreting the $\delta^{44/40}Ca$ values of marine carbonates deposited throughout geologic history.

Conclusions

This study reports Ca isotope data for natural zeolite minerals from Iceland, as well as hydrothermal calcite, bulk basalt, and primary mineral separates. Zeolite minerals display a $\delta^{44/40}Ca$ range of ~1.4‰, which is on the order of the range exhibited by all igneous rocks thus far measured[6,26]. Zeolite $\delta^{44/40}Ca$ values strongly correlate with average Ca–O bond lengths, which we interpret to reflect equilibrium isotope partitioning. The bond-length hypothesis presented here also provides some evidence that equilibrium isotope effects control $\Delta^{44/40}Ca$ between hydrothermal calcite and waters, given that these reservoirs support similar Ca–O bond lengths and display small isotopic offsets. As equilibrium isotope fractionation factors strongly depend on temperature[10], our findings suggest that the Ca isotope geochemistry of zeolite minerals could be developed into an entirely new geothermometer for investigating low-grade basalt

metamorphism. Moreover, zeolites should be considered in Ca isotope studies of other continental and oceanic hydrothermal systems where the minerals pervasively occur. Calcium isotopes hold particular promise for quantifying the mineralization of injected CO_2 during mineral carbonation of basalt, which is a leading CCS strategy[29,30]. Our study characterizes the composition of key mineral reservoirs necessary for interpreting and modeling Ca isotope variations in both field and theoretical CCS studies. More research dedicated to the Ca isotope geochemistry of zeolites could help improve numerous environmental, industrial, and medical applications of the minerals.

Methods

Field collection. During the summer of 2017, zeolites, bulk basalt, and calcite were collected from various outcrops in the Berufjörður–Breiðdalur region of East Iceland. No permissions were required for sampling in this location. Mineral types were identified in the field and later confirmed by X-ray diffraction (XRD), as described below. Where possible, coindex zeolite pairs were collected from a single outcrop for every depth-zone described by Walker (1960), and calcite samples were collected from all zones. Rock samples for primary mineral separates were collected from basaltic flows throughout Iceland (Fig. 1).

Sample preparation. Heavy liquids (Apatite-to-Zircon Inc., Viola, ID, USA) were used to separate mostly pure fractions of plagioclase, clinopyroxene, olivine, and apatite from three basalt samples with different ages and geologic histories. Intergrown zeolite samples from the same amygdule were physically separated. All basalt and mineral specimens, including primary minerals, calcite, and zeolites, were washed with MilliQ water and sonicated to remove excess sediment and impurities. Samples were dried in an oven at 50 °C and powdered by hand using a Diamonite mortar and pestle. Zeolites fundamentally differ from typical rock-forming silicate minerals, as their frameworks only comprise Al, Si, and O, that is, the minerals do not contain structurally bound Ca. All Ca is extra-framework, as it occurs in voids and channels created by the frameworks. Therefore, bulk measurements are most appropriate for characterizing the Ca isotope geochemistry of zeolites. Subsamples of basalt, primary mineral, and zeolite powders were completely digested using HF and HNO_3 acids. No insoluble residues were observed. Calcite powders were completely dissolved in 5% HNO_3. To further interrogate the Ca isotope geochemistry of zeolites, a sequential leaching and digestion procedure was applied. Supplementary information (S2) more completely describes this experiment, and the results are summarized in Table S3 and Fig. S2. The leaching solution clearly fractionated Ca isotopes, as indicated by correlations between $\delta^{44/40}$Ca values and elemental ratios (Fig. S3), as well as fractions of Ca leached (Fig. S4); therefore, leachate and residual digest $\delta^{44/40}$Ca values were excluded from the main interpretations of this study.

X-ray diffraction. The identities of zeolite specimens collected in the field were confirmed by XRD in the Integrated Molecular Structure Education and Research Center at Northwestern University. Powder XRD data were collected at room temperature on an STOE-STADI-P powder diffractometer equipped with an asymmetrically curved germanium monochromator (CuKα1 radiation, $\lambda = 1.54056$ Å) and a one-dimensional silicon strip detector (MYTHEN2 1K from DECTRIS). The line focused Cu X-ray tube was operated at 40 kV and 40 mA. Intensity data from 2θ ranges of 1°–100° were collected over a period of 30 min. The instrument was calibrated against a NIST Si standard (640d) prior to measurement.

Elemental analysis. Sample solutions were diluted with 5% HNO_3 and analyzed for concentrations of Ca, Na, Mg, K, and Sr using a Thermo Scientific iCAP 6500 ICP-OES at Northwestern University. The concentrations have an uncertainty of ±5% (relative standard deviation), as determined by repeated analyses of NIST SRM 1643f. Concentrations of Si and Al were measured using a lithium metaborate fusion procedure and an Enviro II ICP-AES (Activation Laboratories, Ancaster, ON). These data have an uncertainty of ±5%.

Ca isotope ratios. Calcium isotope ratios (^{44}Ca/^{40}Ca) were measured with a Thermo Fisher Triton MC-TIMS in the Radiogenic Isotope Laboratory at Northwestern University, using an optimized ^{43}Ca–^{42}Ca double-spike procedure[135]. Samples containing 50 µg of Ca were equilibrated with the spike, and the solutions were eluted through Teflon columns packed with Bio-Rad AG MP-50 cation-exchange resin. Approximately 12.5 µg of purified Ca was loaded onto outgassed, single Ta filament assemblies together with 0.5 µL of 10% H_3PO_4. Total procedural blanks ($n = 4$) determined with a ^{42}Ca isotope dilution method were negligible (65–117 ng). Reported $\delta^{44/40}$Ca have an internal precision of ±0.02–0.03‰ ($2\sigma_{SEM}$). The double spike was frequently recalibrated by analyzing at least 8 OSIL ASW standards and 2 NIST 915b standards every 30 or fewer samples. During the period of study, repeated analyses of the standards yielded $\delta^{44/40}Ca_{ASW} = 0.000 \pm 0.005$‰ ($2\sigma_{SEM}$, $n = 68$) and $\delta^{44/40}Ca_{915b} = -1.147 \pm 0.012$‰ ($2\sigma_{SEM}$, $n = 17$). These data correspond to a short-term external reproducibility ($2\sigma_{SD}$) of ±0.045‰ for OSIL ASW and ±0.049‰ for NIST 915b. Long-term records for the laboratory yield $\delta^{44/40}Ca_{ASW} = 0.000 \pm 0.002$‰ ($2\sigma_{SEM}$, $n = 661$) and $\delta^{44/40}Ca_{915b} = -1.135 \pm 0.003$‰ ($2\sigma_{SEM}$, $n = 263$). These data point to a $2\sigma_{SD}$ of ±0.044‰ for OSIL ASW and ±0.048‰ for NIST 915b. Based on all standard measurements, we adopt a $2\sigma_{SD}$ of ±0.05‰ for the present dataset. As shown in the data tables, duplicate analyses of sample unknowns are better than ±0.02‰. Long-term records for the laboratory yield an SRM915a value of $\delta^{44/40}Ca_{915a} = -1.86 \pm 0.01$‰ ($2\sigma_{SEM}$, $n = 68$) relative to ASW; therefore, data reported here can be converted to the SRM915a scale using the following equation: $\delta^{44/40}$Ca (‰, SRM915a) = $\delta^{44/40}$Ca (‰, ASW) + 1.86‰.

Bond-length calculation. The weighted average bond length per zeolite mineral (L) was approximated by compiling published data on lengths for the two types of bonds (either Ca–O_w or Ca–O_{fmwk}) specific to each exchange site containing Ca (Table S2). For some zeolites, Ca occupying a given exchange site can coordinate to both water O atoms and framework O atoms (Table 3). Because, in general, bond lengths differ depending on whether Ca coordinates to water O or framework O atoms, we calculated weighted average, site-specific bond lengths (l_s), which account for differences in Ca–O_w bond lengths (l_w) and Ca–O_{fmwk} bond lengths (l_{fmwk}) according to the number of water O atoms (N_w) and framework O atoms (N_{fmwk}) available for coordination.

The equations are:

$$L = (f_{Ca_1} \times l_{s_1}) + (f_{Ca_2} \times l_{s_2}) \cdots + (f_{Ca_i} \times l_{s_i}) \quad (1)$$

$$l_s = \left(l_w \times \frac{N_w}{CN_s}\right) + \left(l_{fmwk} \times \frac{N_{fmwk}}{CN_s}\right) \quad (2)$$

$$CN_s = N_w + N_{fmwk} \quad (3)$$

where L is the estimated bond length per mineral (Å), f_{Ca} is the fraction of Ca occupying each site (1, 2,…i), l_s is the weighted average site-specific bond length (Å), l_w is the average Ca–O_w bond length in a given site (Å), l_{fmwk} is the average Ca–O_{fmwk} bond length in a given site (Å), N_w is the number of Ca–O_w bonds in a given site, N_{fmwk} is the number of Ca–O_{fmwk} bonds in a given site, and CN_s is the coordination number of Ca in a given site.

The calculations adopted for Fig. 4 assume even distribution of Ca across all potential Ca-bearing sites (Table 3). Sensitivity to this assumption was tested by changing f_{Ca} to values that produce the minimum and maximum possible estimates of L for each mineral. The correlation remains significant for all scenarios ($R^2 > 0.80$, $p < 0.001$). See Supplementary information (S1) for more details on statistical analysis (Table S1).

Data availability

The authors declare that all data supporting the findings of this study are available within the paper and its Supplementary information files. Data used to generate Figs. 1–4 can also be found on Dryad (datadryad.org) using the following DOI link https://doi.org/10.5061/dryad.dfn2z352s.

Received: 4 March 2021; Accepted: 10 September 2021;
Published online: 01 October 2021

References

1. Fleischer, M. The abundance and distribution of the chemical elements in the earth's crust. *J. Chem. Educ.* **31**, 446 (1954).
2. Berner, R. A., Lasaga, A. C. & Garrels, R. M. The carbonate-silicate geochemical cycle and its effect on atmospheric carbon dioxide over the past 100 million years. *Am. J. Sci.* **283**, 641–683 (1983).
3. Urey, H. C. On the early chemical history of the Earth and the origin of life. *Proc. Natl Acad. Sci. USA* **38**, 351–363 (1952).
4. DePaolo, D. J. Calcium isotopic variations produced by biological, kinetic, radiogenic and nucleosynthetic processes. *Rev. Mineral. Geochem.* **55**, 255–288 (2004).
5. Gussone, N. et al. *Calcium Stable Isotope Geochemistry* (Springer, 2016).
6. Fantle, M. S. & Tipper, E. T. Calcium isotopes in the global biogeochemical Ca cycle: implications for development of a Ca isotope proxy. *Earth Sci. Rev.* **129**, 148–177 (2014).
7. Griffith, E. M. & Fantle, M. S. Introduction to calcium isotope geochemistry: past lessons and future directions. *Chem. Geol.* **537**, 119470 (2020).
8. Bigeleisen, J. & Mayer, M. G. Calculation of equilibrium constants for isotopic exchange reactions. *J. Chem. Phys.* **15**, 261–267 (1947).
9. Schauble, E. A. Applying stable isotope fractionation theory to new systems. *Rev. Mineral. Geochem.* **55**, 65–111 (2004).

10. Urey, H. C. The thermodynamic properties of isotopic substances. *J. Chem. Soc.* **4**, 562–581 (1947).
11. DePaolo, D. J. Surface kinetic model for isotopic and trace element fractionation during precipitation of calcite from aqueous solution. *Geochim. Cosmochim. Acta* **75**, 1039–1056 (2011).
12. Nielsen, L. C., DePaolo, D. J. & De Yoreo, J. J. Self-consistent ion-by-ion growth model for kinetic isotopic fractionation during calcite precipitation. *Geochim. Cosmochim. Acta* **86**, 166–181 (2012).
13. Tang, J., Dietzel, M., Böhm, F., Köhler, S. J. & Eisenhauer, A. Sr^{2+}/Ca^{2+} and $^{44}Ca/^{40}Ca$ fractionation during inorganic calcite formation: II. Ca isotopes. *Geochim. Cosmochim. Acta* **72**, 3733–3745 (2008).
14. Wang, J., Jacobson, A. D., Sageman, B. B. & Hurtgen, M. T. Stable Ca and Sr isotopes support volcanically triggered biocalcification crisis during Oceanic Anoxic Event 1a. *Geology* **49**, 515–519 (2021).
15. Blättler, C. L., Hong, W.-L., Kirsimäe, K., Higgins, J. A. & Lepland, A. Small calcium isotope fractionation at slow precipitation rates in methane seep authigenic carbonates. *Geochim. Cosmochim. Acta* **298**, 227–239 (2021).
16. AlKhatib, M. & Eisenhauer, A. Calcium and strontium isotope fractionation in aqueous solutions as a function of temperature and reaction rate; I. Calcite. *Geochim. Cosmochim. Acta* **209**, 296–319 (2017).
17. Lemarchand, D., Wasserburg, G. J. & Papanastassiou, D. A. Rate-controlled calcium isotope fractionation in synthetic calcite. *Geochim. Cosmochim. Acta* **68**, 4665–4678 (2004).
18. Marriott, C. S., Henderson, G. M., Belshaw, N. S. & Tudhope, A. W. Temperature dependence of δ 7 Li, δ 44 Ca and Li/Ca during growth of calcium carbonate. *Earth Planet. Sci. Lett.* **222**, 615–624 (2004).
19. Amini, M. et al. Calcium isotope ($\delta^{44/40}Ca$) fractionation along hydrothermal pathways, Logatchev field (Mid-Atlantic Ridge, 14°45′N). *Geochim. Cosmochim. Acta* **72**, 4107–4122 (2008).
20. Brown, S. T., Kennedy, B. M., DePaolo, D. J., Hurwitz, S. & Evans, W. C. Ca, Sr, O and D isotope approach to defining the chemical evolution of hydrothermal fluids: example from Long Valley, CA, USA. *Geochim. Cosmochim. Acta* **122**, 209–225 (2013).
21. Jacobson, A. D., Grace Andrews, M., Lehn, G. O. & Holmden, C. Silicate versus carbonate weathering in Iceland: new insights from Ca isotopes. *Earth Planet. Sci. Lett.* **416**, 132–142 (2015).
22. John, T. et al. Volcanic arcs fed by rapid pulsed fluid flow through subducting slabs. *Nat. Geosci.* **5**, 489–492 (2012).
23. Feng, C., Qin, T., Huang, S., Wu, Z. & Huang, F. First-principles investigations of equilibrium calcium isotope fractionation between clinopyroxene and Ca-doped orthopyroxene. *Geochim. Cosmochim. Acta* **143**, 132–142 (2014).
24. Huang, S., Farkaš, J. & Jacobsen, S. B. Calcium isotopic fractionation between clinopyroxene and orthopyroxene from mantle peridotites. *Earth Planet. Sci. Lett.* **292**, 337–344 (2010).
25. Antonelli, M. A. et al. Kinetic and equilibrium Ca isotope effects in high-T rocks and minerals. *Earth Planet. Sci. Lett.* **517**, 71–82 (2019).
26. Antonelli, M. A. & Simon, J. I. Calcium isotopes in high-temperature terrestrial processes. *Chem. Geol.* **548**, 119651 (2020).
27. Gussone, N., Austrheim, H., Westhues, A. & Mezger, K. Origin of Rodingite forming fluids constrained by calcium and strontium isotope ratios in the Leka Ophiolite Complex. *Chem. Geol.* **542**, 119598 (2020).
28. Brown, S. T. et al. High-temperature kinetic isotope fractionation of calcium in epidosites from modern and ancient seafloor hydrothermal systems. *Earth Planet. Sci. Lett.* **535**, 116101 (2020).
29. Pogge von Strandmann, P. A. E. et al. Rapid CO2 mineralisation into calcite at the CarbFix storage site quantified using calcium isotopes. *Nat. Commun.* **10**, 1–7 (2019).
30. Snæbjörnsdóttir, S. Ó. et al. Carbon dioxide storage through mineral carbonation. *Nat. Rev. Earth Environ.* https://doi.org/10.1038/s43017-019-0011-8 (2020).
31. Chipera, S. J. & Apps, J. A. Geochemical stability of natural zeolites. *Mineral. Soc. Am.* **45**, 117–161 (2001).
32. Coombs, D. S., Ellis, A. J., Fyfe, W. S. & Taylor, A. M. The zeolite facies, with comments on the interpretation of hydrothermal syntheses. *Geochim. Cosmochim. Acta* **17**, 53–107 (1959).
33. Armbruster, T. & Gunter, M. E. Crystal structures of natural zeolites. *Rev. Mineral. Geochem.* **45**, 1–67 (2001).
34. Pabalan, R. T. & Bertetti, F. P. Cation-exchange properties of natural zeolites. *Rev. Mineral. Geochem.* **45**, 453–518 (2001).
35. Passaglia, E. & Sheppard, R. A. The crystal chemistry of zeolites. *Mineral. Soc. Am.* **45**, 69–116 (2001).
36. Franzson, H. Hydrothermal evoution of the Nesjavellir high-temperature system, Iceland. In *Proc. World Geothermal Congress, Japan*, 2075–2080 (2000).
37. Kristmannsdóttir, H. & Tómasson, J. in *Natural Zeolites* (eds Sand, L. B. & Mumpton, F. A.) 227–284 (Oxford, 1978).
38. Neuhoff, P. S., Fridriksson, T. & Arnorsson, S. Porosity evolution and mineral paragenesis during low-grade metamorphism of basaltic lavas at Teigarhorn, eastern Iceland. *Am. J. Sci.* **299**, 467–501 (1999).
39. Neuhoff, P. S., Fridriksson, T. & Bird, D. K. Zeolite parageneses in the North Atlantic Igneous Province: implications for geotectonics and groundwater quality of basaltic crust. *Int. Geol. Rev.* **42**, 15–44 (2000).
40. Weisenberger, T. B., Spürgin, S. & Lahaye, Y. Hydrothermal alteration and zeolitization of the Fohberg phonolite, Kaiserstuhl Volcanic Complex, Germany. *Int. J. Earth Sci.* **103**, 2273–2300 (2014).
41. Weisenberger, T. & Selbekk, R. S. Multi-stage zeolite facies mineralization in the Hvalfjördur area, Iceland. *Int. J. Earth Sci.* **98**, 985–999 (2009).
42. Wood, D. A., Gibson, I. L. & Thompson, R. N. Elemental mobility during zeolite facies metamorphism of the Tertiary basalts of eastern Iceland. *Contr. Mineral. Petrol.* **55**, 241–254 (1976).
43. Fridriksson, T. Experimental determination of thermodynamic properties of ion-exchange in heulandite: binary ion-exchange experiments at 55 and 85 C involving Ca^{2+}, Sr^{2+}, Na^{+}, and K^{+}. *Am. J. Sci.* **304**, 287–332 (2004).
44. Fridriksson, T., Arnórsson, S. & Bird, D. K. Processes controlling Sr in surface and ground waters of Tertiary tholeiitic flood basalts in Northern Iceland. *Geochim. Cosmochim. Acta* **73**, 6727–6746 (2009).
45. Aradóttir, E. S. P., Sonnenthal, E. L., Björnsson, G. & Jónsson, H. Multidimensional reactive transport modeling of CO_2 mineral sequestration in basalts at the Hellisheidi geothermal field, Iceland. *Int. J. Greenhouse Gas Control* **9**, 24–40 (2012).
46. Gysi, A. P. & Stefánsson, A. Experiments and geochemical modeling of CO_2 sequestration during hydrothermal basalt alteration. *Chem. Geol.* **306–307**, 10–28 (2012).
47. Matter, J. M. et al. Rapid carbon mineralization for permanent disposal of anthropogenic carbon dioxide emissions. *Science* **352**, 1312–1314 (2016).
48. Snæbjörnsdóttir, S. Ó. et al. The chemistry and saturation states of subsurface fluids during the in situ mineralisation of CO_2 and H_2S at the CarbFix site in SW-Iceland. *Int. J. Greenhouse Gas Control* **58**, 87–102 (2017).
49. Dessert, C., Dupré, B., Gaillardet, J., François, L. M. & Allègre, C. J. Basalt weathering laws and the impact of basalt weathering on the global carbon cycle. *Chem. Geol.* **202**, 257–273 (2003).
50. Andrews, M. G. & Jacobson, A. D. The radiogenic and stable Sr isotope geochemistry of basalt weathering in Iceland: role of hydrothermal calcite and implications for long-term climate regulation. *Geochim. Cosmochim. Acta* **215**, 247–262 (2017).
51. Rad, S., Allegre, C. & Louvat, P. Hidden erosion on volcanic islands. *Earth Planet. Sci. Lett.* **262**, 109–124 (2007).
52. Li, J., Chang, H., Ma, L., Hao, J. & Yang, R. T. Low-temperature selective catalytic reduction of NO_x with NH_3 over metal oxide and zeolite catalysts—a review. *Catal. Today* **175**, 147–156 (2011).
53. Jiang, N., Shang, R., Heijman, S. G. J. & Rietveld, L. C. High-silica zeolites for adsorption of organic micro-pollutants in water treatment: a review. *Water Res.* **144**, 145–161 (2018).
54. Li, Y., Li, L. & Yu, J. Applications of zeolites in sustainable chemistry. *Chem* **3**, 928–949 (2017).
55. Mumpton, F. A. La roca magica: uses of natural zeolites in agriculture and industry. *Proc. Natl. Acad. Sci. USA* **96**, 3463–3470 (1999).
56. Borai, E. H., Harjula, R., malinen, L. & Paajanen, A. Efficient removal of cesium from low-level radioactive liquid waste using natural and impregnated zeolite minerals. *J. Hazardous Mater.* **172**, 416–422 (2009).
57. Lonin, A. Y., Levenets, V. V., Neklyudov, I. M. & Shchur, A. O. The usage of zeolites for dynamic sorption of cesium from waste waters of nuclear power plants. *J. Radioanal. Nucl. Chem.* **303**, 831–836 (2015).
58. Baek, W., Ha, S., Hong, S., Kim, S. & Kim, Y. Cation exchange of cesium and cation selectivity of natural zeolites: chabazite, stilbite, and heulandite. *Microporous Mesoporous Mater.* **264**, 159–166 (2018).
59. Kallo, D. Applications of natural zeolites in water and wastewater treatment. *Rev. Mineral. Geochem.* **45**, 519–550 (2001).
60. Leyva-Ramos, R. et al. Removal of ammonium from aqueous solution by ion exchange on natural and modified chabazite. *J. Environ. Manage.* **91**, 2662–2668 (2010).
61. Sarshar, Z., Zahedi-Niaki, M. H., Huang, Q., Eić, M. & Kaliaguine, S. MTW zeolites for reducing cold-start emissions of automotive exhaust. *Appl. Catal. B* **87**, 37–45 (2009).
62. Bacakova, L., Vandrovcova, M., Kopova, I. & Jirka, I. Applications of zeolites in biotechnology and medicine – a review. *Biomater. Sci.* **6**, 974–989 (2018).
63. Gussone, N. et al. Calcium isotope fractionation in calcite and aragonite. *Geochim. Cosmochim. Acta* **69**, 4485–4494 (2005).
64. Walker, G. P. L. Zeolite zones and Dike distribution in relation to the structure of the basalts of eastern Iceland. *J. Geol.* **68**, 515–528 (1960).
65. Alfredsson, H. A. et al. The geology and water chemistry of the Hellisheidi, SW-Iceland carbon storage site. *Int. J. Greenhouse Gas Control* **12**, 399–418 (2013).

66. Fridriksson, T., Neuhoff, P. S., Arnórsson, S. & Bird, D. K. Geological constraints on the thermodynamic properties of the stilbite—stellerite solid solution in low-grade metabasalts. *Geochim. Cosmochim. Acta* **65**, 3993–4008 (2001).
67. Kousehlar, M., Weisenberger, T. B., Tutti, F. & Mirnejad, H. Fluid control on low-temperature mineral formation in volcanic rocks of Kahrizak, Iran: fluid control on low-temperature mineral formation. *Geofluids* **12**, 295–311 (2012).
68. White, R. & McKenzie, D. Magmatism at rift zones: the generation of volcanic continental margins and flood basalts. *J. Geophys. Res.* **94**, 7685 (1989).
69. Moorbath, S., Sigurdsson, H. & Goodwin, R. KAr ages of the oldest exposed rocks in Iceland. *Earth Planet. Sci. Lett.* **4**, 197–205 (1968).
70. Robinson, P. T., Mehegan, J., Gibson, I. L. & Schmincke, H.-U. Lithology and structure of the volcanic sequence in eastern Iceland. *J. Geophys. Res.* **87**, 6429–6436 (1982).
71. Walker, G. P. L. Geological investigations in eastern Iceland. *Bull. Volcanol.* **27**, 351–363 (1964).
72. Mehegan, J. M., Robinson, P. T. & Delaney, J. R. Secondary mineralization and hydrothermal alteration in the Reydarfjordur drill core, eastern Iceland. *J. Geophys. Res.* **87**, 6511–6524 (1982).
73. Thien, B. M. J., Kosakowski, G. & Kulik, D. A. Differential alteration of basaltic lava flows and hyaloclastites in Icelandic hydrothermal systems. *Geotherm. Energy* **3**, 11 (2015).
74. Gussone, N., Ahm, A.-S. C., Lau, K. V. & Bradbury, H. J. Calcium isotopes in deep time: potential and limitations. *Chem. Geol.* **544**, 119601 (2020).
75. Ryu, J.-S., Jacobson, A. D., Holmden, C., Lundstrom, C. & Zhang, Z. The major ion, $\delta^{44/40}$Ca, $\delta^{44/42}$Ca, and $\delta^{26/24}$Mg geochemistry of granite weathering at pH=1 and T=25 °C: power-law processes and the relative reactivity of minerals. *Geochim. Cosmochim. Acta* **75**, 6004–6026 (2011).
76. Antonelli, M. A. et al. Ca isotopes record rapid crystal growth in volcanic and subvolcanic systems. *Proc. Natl. Acad. Sci. USA* **116**, 20315–20321 (2019).
77. Zhao, X. et al. Coupled extremely light Ca and Fe isotopes in peridotites. *Geochim. Cosmochim. Acta* **208**, 368–380 (2017).
78. Oelkers, E. H., Pogge von Strandmann, P. A. E. & Mavromatis, V. The rapid resetting of the Ca isotopic signatures of calcite at ambient temperature during its congruent dissolution, precipitation, and at equilibrium. *Chem. Geol.* **512**, 1–10 (2019).
79. Bourg, I. C., Richter, F. M., Christensen, J. N. & Sposito, G. Isotopic mass dependence of metal cation diffusion coefficients in liquid water. *Geochim. Cosmochim. Acta* **74**, 2249–2256 (2010).
80. Hofmann, A. E., Bourg, I. C. & DePaolo, D. J. Ion desolvation as a mechanism for kinetic isotope fractionation in aqueous systems. *Proc. Natl. Acad. Sci. USA* **109**, 18689–18694 (2012).
81. Richter, F. M., Dauphas, N. & Teng, F.-Z. Non-traditional fractionation of non-traditional isotopes: evaporation, chemical diffusion and Soret diffusion. *Chem. Geol.* **258**, 92–103 (2009).
82. Kirov, G. & Filizova, L. Cationic hydration impact on zeolite formation and properties: a review and discussion. *Geochem. Mineral. Petrol.* **49**, 65–82 (2012).
83. Nakamura, H., Okumura, M. & Machida, M. Monte Carlo simulation studies of cation selectivity in ion exchange of zeolites. *RSC Adv.* **4**, 52757–52761 (2014).
84. Donahoe, R. J. & Liou, J. G. An experimental study on the process of zeolite formation. *Geochim. Cosmochim. Acta* **49**, 2349–2360 (1985).
85. Iijima, A. Geology of natural zeolites and zeolitic rocks. *Pure Appl. Chem.* **52**, 2115–2130 (1980).
86. Kiseleva, I., Navrotsky, A., Belitsky, I. & Fursenko, B. Thermochemical study of calcium zeolites—heulandite and stilbite. *Am. Mineral.* **86**, 448–455 (2001).
87. Liou, J. G., de Capitani, C. & Frey, M. Zeolite equilibria in the system $CaAI_2Si_2O_8$-$NaAISi_3O_8$-SiO_2-H_2O. *N. Z. J. Geol. Geophys.* **34**, 293–301 (1991).
88. Liou, J., Maruyama, S. & Cho, A. Phase equilibria and mineral parageneses of metabasites in low-grade metamorphism. *Mineral. Mag.* **49**, 321–333 (1985).
89. Weisenberger, T. & Bucher, K. Mass transfer and porosity evolution during low temperature water–rock interaction in gneisses of the simano nappe: Arvigo, Val Calanca, Swiss Alps. *Contrib. Mineral. Petrol.* **162**, 61–81 (2011).
90. Clark, D. E. et al. Experimental observations of CO_2-water-basaltic glass interaction in a large column reactor experiment at 50 °C. *Int. J. Greenhouse Gas Control* **89**, 9–19 (2019).
91. Armbruster, T. Dehydration mechanism of clinoptilolite and heulandite: single-crystal X-ray study of Na-poor, Ca-, K-, Mg-rich clinoptilolite at 100 K. *Am. Mineral.* **78**, 260–264 (1993).
92. Barrer, R. M. & Klinowski, J. Influence of framework charge density on ion-exchange properties of zeolites. *J, Chem. Soc. Faraday Trans.* **68**, 1956 (1972).
93. Gunter, M. E., Armbruster, T., Kohler, T. & Knowles, C. R. Crystal structure and optical properties of Na- and Pb- exchanged heulandite-group zeolites. *Am. Mineral.* **79**, 675–682 (1994).
94. Zhang, R., Nash, C. P. & Rock, P. A. Thermodynamics of calcium-isotope-exchange reactions. I. Exchange between isotopic calcium carbonates and aqueous calcium ions. *J. Phys. Chem.* **92**, 3989–3993 (1988).
95. Colla, C. A., Wimpenny, J., Yin, Q.-Z., Rustad, J. R. & Casey, W. H. Calcium-isotope fractionation between solution and solids with six, seven or eight oxygens bound to Ca(II). *Geochim. Cosmochim. Acta* **121**, 363–373 (2013).
96. Moynier, F. & Fujii, T. Calcium isotope fractionation between aqueous compounds relevant to low-temperature geochemistry, biology and medicine. *Sci. Rep.* **7**, 44255 (2017).
97. Rustad, J. R. et al. Isotopic fractionation of Mg^{2+}(aq), Ca^{2+}(aq), and Fe^{2+}(aq) with carbonate minerals. *Geochim. Cosmochim. Acta* **74**, 6301–6323 (2010).
98. Wenzhong, W. et al. Concentration effect on equilibrium fractionation of Mg-Ca isotopes in carbonate minerals: insights from first-principles calculations. *Geochim. Cosmochim. Acta* **208**, 185–197 (2017).
99. Chacko, T., Cole, D. R. & Horita, J. Equilibrium oxygen, hydrogen and carbon isotope fractionation factors applicable to geologic systems. *Rev. Mineral. Geochem.* **43**, 1–81 (2001).
100. Alberti, A., Galli, E., Vezzalini, G., Passaglia, E. & Zanazzi, P. F. Position of cations and water molecules in hydrated chabazite. Natural and Na-, Ca-, Sr- and K-exchanged chabazites. *Zeolites* **2**, 303–309 (1982).
101. Lammers, L. N., Kulasinski, K., Zarzycki, P. & DePaolo, D. J. Molecular simulations of kinetic stable calcium isotope fractionation at the calcite-aqueous interface. *Chem. Geol.* **532**, 119315 (2020).
102. Kol'tsova, T. N. Scolecite-mesolite transition in relation to sodium substitution for calcium. *Inorg. Mater.* **46**, 187–195 (2010).
103. Artioli, G., Smith, J. V. & Pluth, J. J. X-ray structure refinement of mesolite. *Acta Crystallogr.* **C42**, 937–942 (1986).
104. Kirfel, A. & Gibbs, G. V. Electron density distributions and bonded interactions for the ®brous zeolites natrolite, mesolite and scolecite and related materials. *Phys. Chem. Miner.* **27**, 270–284 (2000).
105. Ståhl, K. & Thomasson, R. The dehydration and rehydration processes in the natural zeolite mesolite studied by conventional and synchrotron X-ray powder diffraction. *Zeolites* **14**, 12–17 (1994).
106. Wang, W., Qin, T., Zhou, C., Huang, S., Wu, Z. & Huang, F. Concentration effect on equilibrium fractionation of Mg-Ca isotopes in carbonate minerals: Insights from first-principles calculations. *Geochimica et Cosmochimica Acta.* **208**, 185–197 (2017).
107. Aufort, J. et al. Site-specific equilibrium isotopic fractionation of oxygen, carbon and calcium in apatite. *Geochim. Cosmochim. Acta* **219**, 57–73 (2017).
108. Griffith, E. M., Schauble, E. A., Bullen, T. D. & Paytan, A. Characterization of calcium isotopes in natural and synthetic barite. *Geochim. Cosmochim. Acta* **72**, 5641–5658 (2008).
109. Chen, C. et al. Compositional and pressure controls on calcium and magnesium isotope fractionation in magmatic systems. *Geochim. Cosmochim. Acta* **290**, 257–270 (2020).
110. Taylor, T. I. & Urey, H. C. Fractionation of the lithium and potassium isotopes by chemical exchange with zeolites. *J. Chem. Phys.* **6**, 429–438 (1938).
111. Hay, R. L. & Sheppard, R. A. Occurrence of zeolites in sedimentary rocks: an overview. *Rev. Mineral. Geochem.* **45**, 217–234 (2001).
112. Lisitzina, N. A. & Butuzova, G. Y. Authigenic zeolites in the sedimentary mantle of the world ocean. *Sediment. Geol.* **31**, 33–41 (1982).
113. Gysi, A. P. & Stefánsson, A. Mineralogical aspects of CO_2 sequestration during hydrothermal basalt alteration—an experimental study at 75 to 250 °C and elevated pCO_2. *Chem. Geol.* **306–307**, 146–159 (2012).
114. Gysi, A. P. & Stefánsson, A. Numerical modelling of CO_2-water-basalt interaction. *Mineral. Mag.* **72**, 55–59 (2008).
115. Weisenberger, T. B., Ingimarsson, H., Hersir, G. P. & Flóvenz, Ó. G. Cation-exchange capacity distribution within hydrothermal systems and its relation to the alteration mineralogy and electrical resistivity. *Energies* **13**, 5730 (2020).
116. Flaathen, T. K., Gislason, S. R., Oelkers, E. H. & Sveinbjörnsdóttir, Á. E. Chemical evolution of the Mt. Hekla, Iceland, groundwaters: a natural analogue for CO_2 sequestration in basaltic rocks. *Appl. Geochem.* **24**, 463–474 (2009).
117. Gislason, S. R. & Arnórsson, S. Dissolution of primary basaltic minerals in natural waters: saturation state and kinetics. *Chem. Geol.* **105**, 117–135 (1993).
118. Pogge von Strandmann, P. A. E. et al. The effect of hydrothermal spring weathering processes and primary productivity on lithium isotopes: Lake Myvatn, Iceland. *Chem. Geol.* **445**, 4–13 (2016).
119. Thomas, D. L., Bird, D. K., Arnórsson, S. & Maher, K. Geochemistry of CO_2-rich waters in Iceland. *Chem. Geol.* **444**, 158–179 (2016).
120. Hindshaw, R. S., Bourdon, B., Pogge von Strandmann, P. A. E., Vigier, N. & Burton, K. W. The stable calcium isotopic composition of rivers draining basaltic catchments in Iceland. *Earth Planet. Sci. Lett.* **374**, 173–184 (2013).
121. Druhan, J. L., Steefel, C. I., Williams, K. H. & DePaolo, D. J. Calcium isotope fractionation in groundwater: molecular scale processes influencing field scale behavior. *Geochim. Cosmochim. Acta* **119**, 93–116 (2013).
122. Syverson, D. D., Scheuermann, P., Higgins, J. A., Pester, N. J. & Seyfried, W. E. Experimental partitioning of Ca isotopes and Sr into anhydrite: consequences for the cycling of Ca and Sr in subseafloor mid-ocean ridge hydrothermal systems. *Geochim. Cosmochim. Acta* **236**, 160–178 (2018).
123. Utada, M. Zeolites in burial diagenesis and low-grade metamorphic rocks. *Rev. Mineral. Geochem.* **45**, 277–304 (2001).

124. Mayfield, K. K. et al. Groundwater discharge impacts marine isotope budgets of Li, Mg, Ca, Sr, and Ba. *Nat. Commun.* **12**, 148 (2021).
125. Jacobson, A. D. & Holmden, C. δ^{44}Ca evolution in a carbonate aquifer and its bearing on the equilibrium isotope fractionation factor for calcite. *Earth Planet. Sci. Lett.* **270**, 349–353 (2008).
126. Fantle, M. S. & DePaolo, D. J. Ca isotopes in carbonate sediment and pore fluid from ODP Site 807A: the Ca^{2+}(aq)–calcite equilibrium fractionation factor and calcite recrystallization rates in Pleistocene sediments. *Geochim. Cosmochim. Acta* **71**, 2524–2546 (2007).
127. Mills, J. V., DePaolo, D. J. & Lammers, L. N. The influence of Ca:CO_3 stoichiometry on Ca isotope fractionation: implications for process-based models of calcite growth. *Geochim. Cosmochim. Acta* **298**, 87–111 (2021).
128. Reeder, R. J. *Carbonates: Mineralogy and Chemistry*, Vol. 11 (Mineralogical Society of America, 1983).
129. Smyth, J. R. & Ahrens, T. J. The crystal structure of calcite III. *Geophys. Res. Lett.* **24**, 1595–1598 (1997).
130. Skinner, J. & Jansen, H. Structure and bonding of calcite: a theoretical study. *Am. Mineral.* **79**, 205–214 (1994).
131. Hewish, N. A., Neilson, G. W. & Enderby, J. E. Environment of Ca^{2+} ions in aqueous solvent. *Nature* **297**, 138–139 (1982).
132. Todorova, T., Hünenberger, P. H. & Hutter, J. Car–Parrinello molecular dynamics simulations of $CaCl_2$ aqueous solutions. *J. Chem. Theory Comput.* **4**, 779–789 (2008).
133. Lim, L. H. V., Pribil, A. B., Ellmerer, A. E., Randolf, B. R. & Rode, B. M. Temperature dependence of structure and dynamics of the hydrated Ca^{2+} ion according to ab initio quantum mechanical charge field and classical molecular dynamics. *J. Comput. Chem.* **31**, 1195–1200 (2009).
134. Katz, A. K., Glusker, J. P., Beebe, S. A. & Bock, C. W. Calcium ion coordination: a comparison with that of beryllium, magnesium, and zinc. *J. Am. Chem. Soc.* **118**, 5752–5763 (1996).
135. Lehn, G. O., Jacobson, A. D. & Holmden, C. Precise analysis of Ca isotope ratios ($\delta^{44/40}$Ca) using an optimized 43Ca–^{42}Ca double-spike MC-TIMS method. *Int. J. Mass Spectrom.* **351**, 69–75 (2013).
136. Markgraf, S. A. & Reeder, R. J. High-temperature structure refinements of calcite and magnesite. *American Mineralogist*. **70**, 590–600 (1985).

Acknowledgements

Special thanks to M. Gasser, C. Feucht, and H. Dijkstra for help with field collection, M. Ankney and M. Wood for help with laboratory work, and F. Albarède and M.G. Andrews for insightful discussions. Three reviewers provided thoughtful feedback that improved the manuscript. This work was supported by NSF-EAR 1613359 awarded to A.D.J.

Author contributions

C.J.N. conducted fieldwork, carried out laboratory analyses, interpreted the data, and wrote the manuscript. A.D.J. contributed to data interpretation and helped write the manuscript. G.D.K. contributed to data interpretation, edited the manuscript, and conducted statistical analyses and data visualization. T.B.W. provided support during fieldwork, contributed to data interpretation, and edited the manuscript.

Competing interests

The authors declare no competing interests.

Additional information

Supplementary information The online version contains supplementary material available at https://doi.org/10.1038/s43247-021-00274-9.

Correspondence and requests for materials should be addressed to Claire J. Nelson.

Peer review information *Communications Earth & Environment* thanks the anonymous reviewers for their contribution to the peer review of this work. Primary Handling Editor: Joe Aslin.

Reprints and permission information is available at http://www.nature.com/reprints

Publisher's note Springer Nature remains neutral with regard to jurisdictional claims in published maps and institutional affiliations.

Open Access This article is licensed under a Creative Commons Attribution 4.0 International License, which permits use, sharing, adaptation, distribution and reproduction in any medium or format, as long as you give appropriate credit to the original author(s) and the source, provide a link to the Creative Commons license, and indicate if changes were made. The images or other third party material in this article are included in the article's Creative Commons license, unless indicated otherwise in a credit line to the material. If material is not included in the article's Creative Commons license and your intended use is not permitted by statutory regulation or exceeds the permitted use, you will need to obtain permission directly from the copyright holder. To view a copy of this license, visit http://creativecommons.org/licenses/by/4.0/.

© The Author(s) 2021